Materials & Design 221 (2022) 110996

Contents lists available at ScienceDirect

Materials & Design

journal homepage: www.elsevier.com/locate/matdes

Interphase elastic properties of carbon nanotube-epoxy composites and their application in multiscale analysis

Zhaobo Song [a], Yunlong Li [a,c,*], Alberto Carpinteri [a,b], Shijie Wang [c], Bin Yang [c]

[a] Department of Civil and Environmental Engineering, Shantou University, Shantou, Guangdong 515063, China
[b] Department of Structural, Geotechnical and Building Engineering, Politecnico di Torino, 10129 Torino, Italy
[c] Department of Mechanical Engineering, Shenyang University of Technology, Shenyang, Liaoning 110870, China

HIGHLIGHTS

- The interfacial vacuum layer of the CNT/epoxy composite is regarded as a transversely isotropic continuum.
- Systematic methods are provided for measuring the elastic constants of the interfacial vacuum layer between carbon nanotubes and epoxy in molecular dynamics simulation.
- It is found that the out-of-plane shear modulus of the interfacial vacuum layer of the CNT/epoxy composite is very small compared with the modulus in other directions.
- Three-dimensional finite element models of randomly distributed representative volume element containing transverse isotropic interphases are developed.

GRAPHICAL ABSTRACT

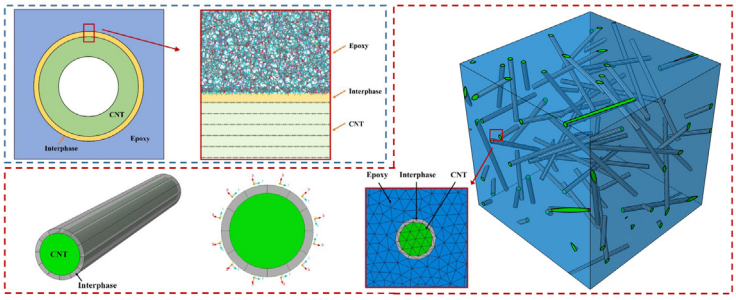

ARTICLE INFO

Article history:
Received 14 March 2022
Revised 26 July 2022
Accepted 26 July 2022
Available online 28 July 2022

Keywords:
Carbon nanotube
Epoxy resin
Interphase layer
Multiscale analysis
Representative volume element

ABSTRACT

A multiscale framework was developed to predict the elastic properties of carbon nanotube (CNT)–epoxy composites. The interfacial vacuum layer between the CNTs and epoxy was equivalent to transversely isotropic elastomer. The elastic constants were calibrated based on the interaction energy density in the molecular dynamics simulations; the results exhibited significant differences between these constants. The out-of-plane shear modulus (46.64 MPa) is four orders of magnitude smaller than the in-plane Young's modulus (362.68 GPa). Subsequently, representative volume elements containing transversely isotropic interphases were developed using the finite element method and analysed comparatively to models without interphases. The results indicated that their difference in the Young's modulus enhancement ratio was sensitive to the CNT aspect ratio. The enhancement ratio of the model containing the interphase was lower when the CNT aspect ratio exceeded a certain value. This difference increased with increasing CNT aspect ratio and was significant at high CNT aspect ratios (7.35 % when the aspect ratio reached 30). In addition, shear-lag analysis indicated that the interphase increased the interfacial load transfer length. This framework provides efficient interfacial simulations, giving a more accurate prediction of bulk elastic properties and can be extended to a wider range of nanocomposites.

* Corresponding author at: Department of Civil and Environmental Engineering, Shantou University, Shantou, Guangdong 515063, China.
E-mail address: li_yunlong3390@163.com (Y. Li).

https://doi.org/10.1016/j.matdes.2022.110996
0264-1275/

1. Introduction

Nanofillers such as nanoparticles, nanotubes, and nanosheets have broad application prospects in polymer composites. These composites exhibit multifunctional characteristics, including mechanical, piezoelectric, and conductive properties [1–4]. Among these nanofillers, carbon nanotubes (CNTs) are extensively used because of their high specific surface area, light weight, and outstanding mechanical, electronic, and thermal properties [5]. When the CNTs fraction is small, a substantial improvement in multifunctional properties is observed in polymer nanocomposites, known as the percolation threshold [6,7]. Effective and precise prediction of the bulk properties of nanocomposites based on CNT fillers is vital for the development of their design and engineering technology. In addition, nanofillers have a higher specific surface area than macroscale fillers, forcing the interface to play a significant role in the bulk mechanical properties and electrical conductivity of nanocomposites [8,9]. By considering the interphase and interface, the prediction of nanocomposites is significantly more precise than when the interphase and interface are absent [10]. Furthermore, the bulk properties of nanocomposites are significantly affected by their interfacial load-transfer efficiency [11]. Thus, the measurement of interface properties is a significant concern.

Experimental methods for the direct measurement of interphase and interface properties are limited owing to technical difficulties in the manipulation of nano-scales. Theoretical approaches have been applied to study the interphases and interfaces. Simple theoretical models for mechanical properties have been developed to measure the properties of the interphase in nanocomposites. In these studies, several models for Young's modulus and tensile strength were used to characterise the thickness, modulus, and strength of the interphase using experimental data [12–14]. Several studies have also considered multi-layered interphases in polymer nanocomposites, in which each layer has unique properties. The strength of each interphase layer was expressed as linear, exponential, and power functions of the distance between the nanoparticles and polymer matrix. Zare et al. [15–17] determined that a power function performs best and predictions of nanocomposites significantly depend on an exponent as a 'Z' factor which demonstrates the level of interphase properties. The surfaces of CNTs cannot provide strong interfacial adhesion with the polymer matrix, which restricts effective load transfer from the matrix to the filler [18]. Zare et al. [19] developed the Hui–Shia model assuming imperfect stress transfer in clay and polymer nanocomposites, the minimum length of platelets required for efficient stress transfer, and interfacial shear strength.

Molecular dynamics (MD) simulations are extensively employed owing to their advantages of precise and transparent reporting of microscale information. Xiong and Meguid [20] investigated the interfacial mechanical characteristics of CNT-reinforced epoxy composites via MD simulations. An interfacial shear strength (ISS) of 40.68 MPa was determined using pull-out tests. Lv et al. [21] investigated the effect of single adatom (SA) and Stone-Wales (SW) defects on the interfacial properties of CNT/polypropylene (PP) composites using MD simulations. The ISS of the SA- and SW-defected CNT/PP composites decreased and increased, respectively, with increasing defect degree. Song et al. [22] further investigated the interfacial properties of amino-functionalised CNT/epoxy composites using pull-out tests and MD simulations. They considered the crosslinks between the amino groups on the CNT and epoxy matrix. It was subsequently determined that by introducing amino groups into the CNTs, the ISS increased by approximately 57 times. In addition, MD simulations can predict the overall macroscopic mechanical properties of composites based on the representative volume element (RVE) concept. At the macroscale, each point of the material sample corresponds to the centre of an RVE, which is sufficiently large to adequately represent the heterogeneities at the microscale, but also sufficiently small with respect to the dimensions of the body [23]. Rahimian-Koloor et al. [24] studied the mechanical behaviour of epoxy-based composites in the presence of single-walled carbon nanotubes (SWCNTs) containing Thrower-Stone-Wales and vacancy defects. Continuous SWCNTs, as long nanofibres, have been considered to constitute nanocomposite RVE. Li et al. [25] performed tension tests to examine the fracture properties of CNT/epoxy composites using MD simulations. The results indicated that the tensile strength and elongation at failure of the CNT/epoxy composites increased by 24.8 and 34.3 %, respectively, compared to those of the unreinforced epoxy matrix. In these studies, MD simulations were useful for investigating the interfacial properties. However, the prediction of the overall properties of composites is limited by the simplistic RVE hypothesis, which states that only one CNT with a low aspect ratio is unidirectionally distributed in the matrix. RVEs containing numerous CNTs with real dimensions and random distributions are still challenging to simulate and analyse. This was ascribed to the longer computing time required for the larger molecular systems.

It is beneficial to apply multiscale approaches to calculate the overall properties of nanocomposites in the presence of an interphase, combining multiple methods across all scales [26,27]. For example, 'fuzzy fibre' reinforced composites in which CNTs are radially grown on the outer circumferential surface of the carbon fibre can be studied comprehensively using multiscale approaches. Kundalwal et al. [28] first estimated the effective elastic properties of a CNT-reinforced polymer matrix nanocomposite (PMNC) using the three-phase Mori–Tanaka model. The interfacial vacuum layer between the CNTs and the matrix in the PMNC was treated as an elastic continuum. The PMNC was then treated as a new interphase and incorporated into a scale-up three-phase shear-lag model of the 'fuzzy fibre' reinforced composite, considering the staggering effect. Kundalwal and Meguid [29] studied the thermomechanical response of 'fuzzy fibre' reinforced composites using multiscale approaches. The Mori–Tanaka model was employed to estimate the properties of the nanofibre consisting of CNTs and an interfacial vacuum layer. Subsequently, considering the nanofibre as the reinforcement and the polymer matrix as the matrix phase, the Mori–Tanaka model was augmented to estimate the properties of the unwound PMNC. Finally, considering the PMNC as the matrix and the fibre as the reinforcement, the Mori–Tanaka model on the largest scale was used to derive the properties of 'fuzzy fibre' reinforced composites. Furthermore, the interfacial and mechanical properties of CNT-reinforced epoxy composites can be characterised using multiscale approaches [30]. First, the interfacial and mechanical properties of small-scale RVE-containing CNTs embedded in epoxy were determined via MD simulations. Then, considering the small-scale RVE as the reinforcement and the epoxy as the matrix phase, the bulk elastic properties of the nanocomposite were determined using the Mori–Tanaka model on a large scale.

In multiscale approaches, the finite element method (FEM) is typically employed to simulate the RVE on a large scale and decrease the number of calculations. Doagou-Rad et al. [31] developed a finite-element RVE embedded in realistic morphology-based microstructures including CNTs and graphene sheets. The elastic constitutive relationship of the nanofillers was characterised using MD simulations. Moreover, the interfacial load transfer in CNT-epoxy composites is weak and mainly carried by van der Waals (vdW) forces. By assuming a perfect interfacial bond, they overlooked the interfacial load transfer efficiency between the micro-components and matrix. Zaccardi [32] evaluated the elastic properties of CNT-epoxy nanocomposites via a 3D multiscale FEM model of RVE. The vdW interactions were used to establish a cohesive law for the zero-thickness interface, which was implemented

using the cohesive zone model (CZM). However, introducing a nonlinear CZM requires time-consuming calculations, and convergence may be difficult. This opens up the possibility of developing simpler and more efficient models. Fankhänel et al. [33] investigated the interphase properties of boehmite nanoparticle (BNP)/epoxy composites via MD simulations. Subsequently, a 3D FEM model of the RVE was constructed in the presence of the interphase. Although the local region in the matrix (where the properties change) was defined as the interphase, the weak vdW interaction region at the interface was not investigated. Consequently, it was treated as a perfect bond in the FEM models, resulting in an overestimation of the interfacial load transfer efficiency. In conclusion, the definitions and constitutive relationship measurement methods of the interface or interphase, which are required for FEM simulations, are challenging to determine accurately and remain an unsolved problem.

To effectively and accurately define the interphase and interface of the nanocomposites, it is necessary to assess them at the atomic scale. Fankhänel et al. [33] observed fewer stiffness changes in the matrix near nanoparticles with no interfacial covalent bonding. The mechanical properties of nanocomposites affected by a region of property change in the matrix may be insignificant compared to the interfacial non-bonded region (interfacial vacuum layer). Moreover, because interfacial load transfer is directly carried by non-bonded vdW interactions, it is essential to comprehensively check the interfacial non-bonded region. One effective approach is to treat this region as a solid continuum, similar to how CNTs are always treated as solid cylinders, even though there are hollow vacuum regions in CNTs. Finally, the correct constitutive relations for these approximations were obtained. Arash et al. [34] equated the interfacial non-bonded region of CNT/polymer composites with an elastic continuum of nonzero thickness. The effective Young's modulus of the interfacial region in the direction parallel to the interface was calculated as the second derivative of the interaction energy between the CNT and the matrix with respect to the applied strains using MD simulations. However, the assumption of isotropic interfacial properties can be inaccurate. This can be assessed by referring to the study conducted by Sahraei et al. [35]. They investigated the interfacial mechanical behaviour of graphene/epoxy nanocomposites by performing normal and sliding pull-out tests. Their study exhibited significant differences in traction–separation curves for the interfacial normal and sliding modes, including the initial slope of the curve (interfacial stiffness) and maximum traction. Thus, the interfacial non-bonded region should be treated as an anisotropic elastic medium that combines a similar structure between CNTs and graphene sheets. In addition, it was determined that the chirality of the CNTs had little influence on the interface interaction during the pull-out test [36,37]. Thus, the anisotropy of the elastic properties can be simplified by transverse isotropy, in which the transversely isotropic plane is parallel to the interface. Based on this understanding of the non-bonded interfacial region, the volume fraction of all the phases can be calculated consistently by considering the nonzero thickness of the interphase. However, it is challenging to directly characterise the constitutive relation of the interface region in tensile and shear tests because of the complex hollow cylindrical shape of the interface region.

This study aims to provide a multiscale framework by focusing only on the interfacial non-bonded region, proposing methods for calibrating the effective transversely isotropic property of the interfacial non-bonded region (interphase) of CNT/polymer composites via MD simulations, and reveal the effects of the interphase on the FEM models of the RVE. 3D FEM models of RVE with randomly distributed CNTs in the presence of the interphase were developed. The effective Young's moduli of the RVE models containing one interphase were calculated at different concentrations and aspect ratios of CNTs and compared with the perfect-bond interface condition. In addition, to explore the load-transfer mechanism in the interphase, three-phase shear-lag models were generated using FEM in the presence of the interphase. The results were then compared with the perfect-bond interface conditions.

2. Calibrations of CNT-epoxy interphase using MD simulations

Owing to the similar structures of CNTs and graphene, graphene sheets are considered as CNTs for investigating the interfacial properties [35,38–41]. In addition, Li and Seidel [40] investigated the effects of graphene curvature and temperature on the interfacial force-separation response of polyethylene matrix composites. The results indicated near identical trends and peak values for different curvatures. Thus, it is scientifically correct to consider the graphene-epoxy interphase as a representative element of the CNT-epoxy interphase. This concept is illustrated in Fig. 1.

In the MD simulations, a polymer-consistent force field (PCFF) was selected to describe the interactions between the atoms. This force field was confirmed to be accurate and has been widely used to simulate CNT-polymer systems [20,35,42].

2.1. Molecular interphase models

Molecular modelling and crosslinking were performed using the BIOVIA Materials Studio 8.0. An epoxy containing diglycidyl ether bisphenol A (DGEBA) resin and diethylenetriamine (DETA) curing agent, as shown in Fig. 2, was employed as the uncrosslinked matrix material. Subsequently, boxes were constructed

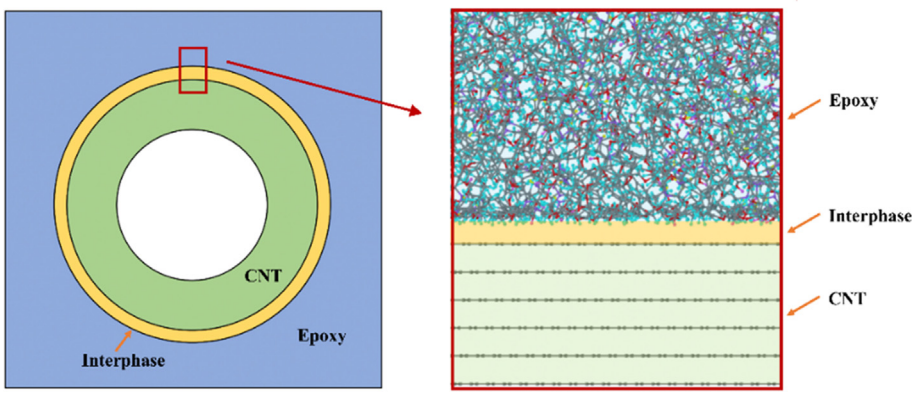

Fig. 1. Sketch of the representative element of the CNT-epoxy interphase.

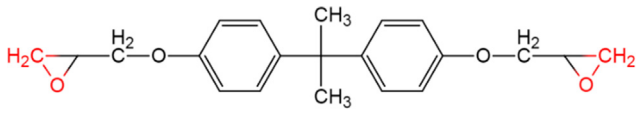

(a) Diglycidyl ether bisphenol A (DGEBA)

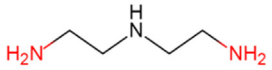

(b) Diethylenetriamine (DETA)

Fig. 2. Molecular structures of: (a) diglycidyl ether bisphenol A (DGEBA) monomer, and (b) diethylenetriamine (DETA) curing agent.

with dimensions of 46.02 × 46.14 × 50.4 Å^3 containing periodic multilayer graphene sheets, with six layers at the bottom of the box. The interlayer spacing of the graphene sheets was 3.4 Å. Several DGEBA and DETA molecular chains were randomly packed into boxes at a ratio of 2:1 with a density of 1.13 g/cm^3. The number of atoms was 11506. The constructed model was subjected to energy minimisation and dynamic relaxation for 500 ps in a constant number, volume, and temperature (NVT) ensemble at 300 K. After equilibration, the model was subjected to annealing crosslinking [22], as shown in Fig. 3. The chemical reactions that occur during the crosslinking process are shown in Fig. 4. One amine group could be crosslinked with two epoxy groups. After the crosslinking process, the model achieved the final degree of crosslinking (92.7 %). The molecular model is shown in Fig. 5.

After crosslinking, the crosslinked models were changed to a large-scale atomic/molecular massively parallel simulator (LAMMPS). The model was subjected to three annealing cycles to obtain a full equilibrium state. The temperature was increased from 300 to 600 K at a heating rate of 1 K/ps in an NVT ensemble. Subsequently, the model was relaxed in an NVT ensemble at 300 K for 1 ns. To obtain a reasonable density, the model was relaxed in a constant number, pressure, and temperature (NPT) ensemble at

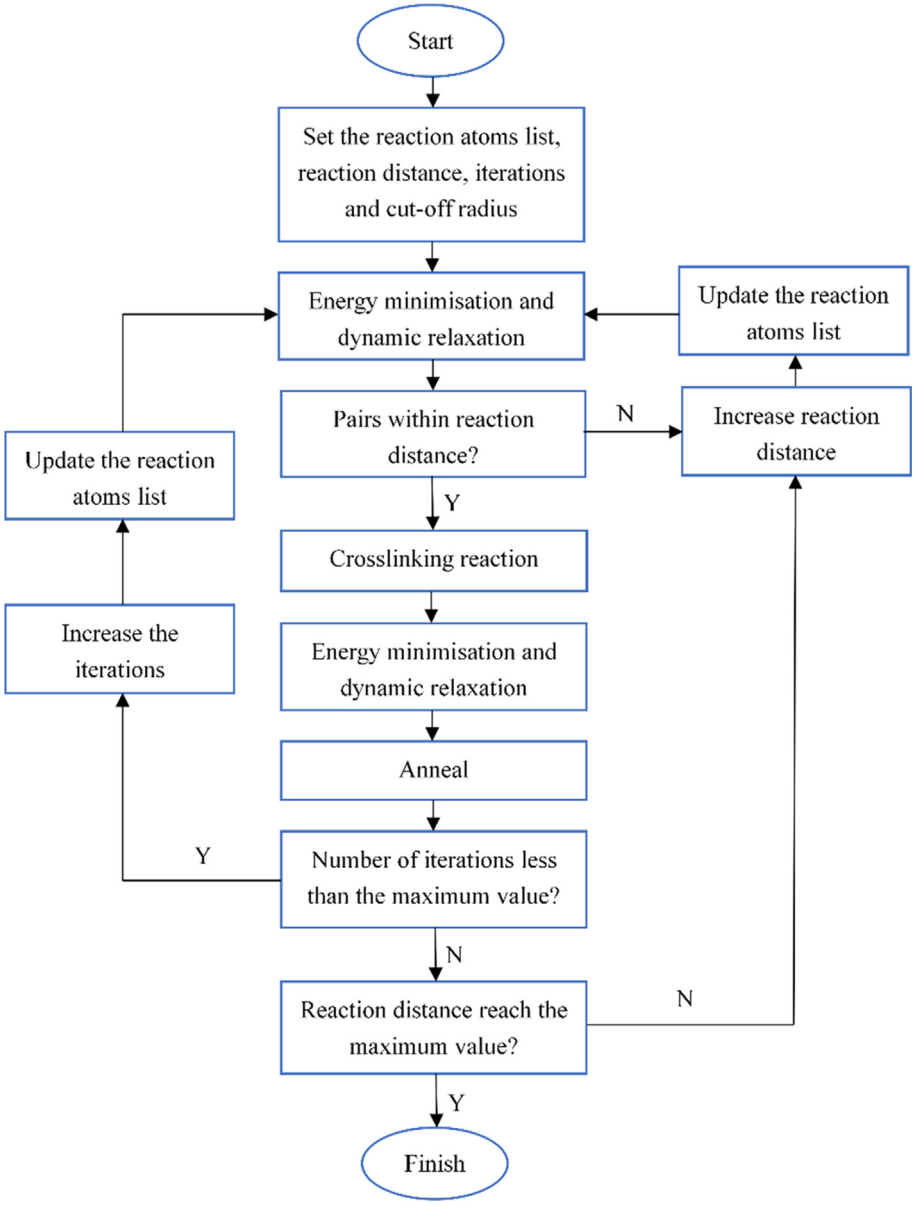

Fig. 3. Crosslinking flowchart [22].

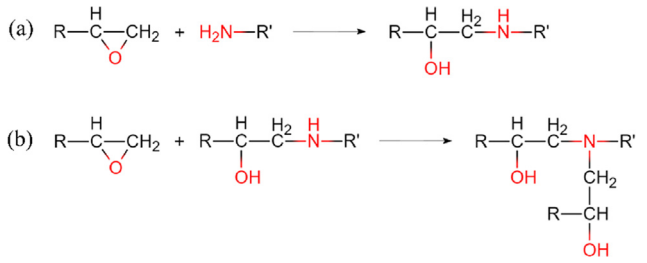

Fig. 4. Two chemical reactions in crosslinking process: (a) epoxy group with primary amine and (b) epoxy group with secondary amine.

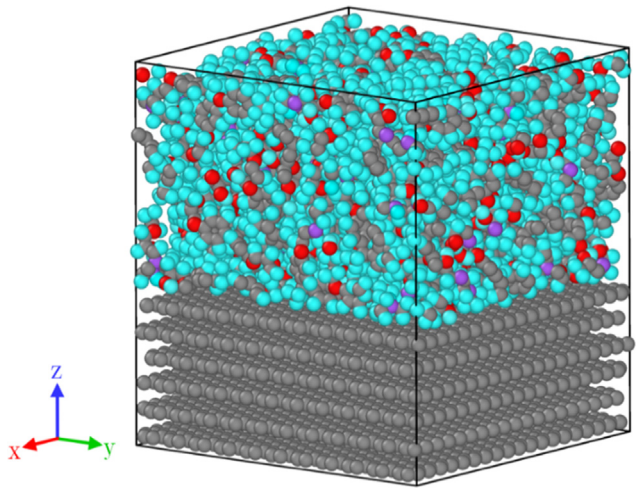

Fig. 5. Molecular model of the CNT-epoxy composite. The grey, blue, cyan, and red colours denote carbon, nitrogen, hydrogen, and oxygen, respectively.

300 K and 1 atm for 1 ns. Finally, the model was subjected to an NVT ensemble at 300 K for 1 ns. As described above, a separate equilibrium procedure was required for the two types of models with different boundary conditions to perform engineering elastic constant tests. One model had periodic conditions in all directions, whereas the other changed the periodic boundary condition to a nonperiodic boundary condition perpendicular to the surface of the graphene sheet, as shown in Fig. 6.

2.2. Elastic properties of interphase

Arash et al. [34] equated the interfacial non-bonded region of CNT/polymer composites with an isotropic elastic continuum. However, the assumption of isotropic interfacial properties may be inaccurate. This interphase can exhibit anisotropic elastic properties. In addition, pull-out tests have shown that the chirality of CNTs has little influence on the interface interactions [36,37]. Thus, the interphase region is treated as a transversely isotropic elastic continuum. The thickness of the interphase was assumed to be 3 Å, based on the vdW equilibrium distance in this interfacial region. The models were illustrated using the Cartesian coordinate system, *xyz*. The *z*-axis represents the axis of elastic symmetry perpendicular to the surface of the graphene sheet, whereas the yz-axis represents the transverse plane. The effective elastic constant can be calculated as follows:

$$C_{ijkl} = \frac{\partial^2 W}{\partial \varepsilon_{ij} \partial \varepsilon_{kl}} \tag{1}$$

where C_{ijkl} and ε_{ij} denote the effective elastic constant and strain tensor, respectively. W denotes the strain energy density, which is a function of the strain components. The strain energy variations in the interphase and the equivalent solid continuum were assumed to be the same. Accordingly, continuum-based relations were used to determine the elastic constants. For the interphase, the variation in strain energy can be substituted by the variation in the interaction energy in MD simulations [34]. The interaction energy is the difference between the total potential energy of the composite and sum of the potential energies of the individual components:

$$U_{inter} = U_{total} - (U_{CNT} + U_{epoxy}) \tag{2}$$

where U_{total} is the total potential energy of the composite, U_{CNT} is the potential energy of the CNT reinforcements, and U_{epoxy} is the potential energy of the polymer matrix.

Five individual engineering elastic constants are required to describe the transversely isotropic elastic constitutive relation. For ease of calculation, they were chosen as follows: in-plane Young's modulus (E_2), out-of-plane Young's modulus (E_3), in-plane shear modulus (G_{12}), out-of-plane shear modulus (G_{13}), and Poisson's ratio for tension stress in the y-direction (υ_{23}). Because the vdW equilibrium distance between the CNTs and polymer matrix remained unchanged during the stretching of the interphase in the x-direction, υ_{23} was assumed to be zero. Therefore, four loading strategies are used for the remaining four elastic moduli. For specific stress or strain conditions, only one of these moduli appears in the strain-energy density function. All loading simulations were implemented using an NVT ensemble. The tests were repeated five times for each loading scenario and the results were averaged.

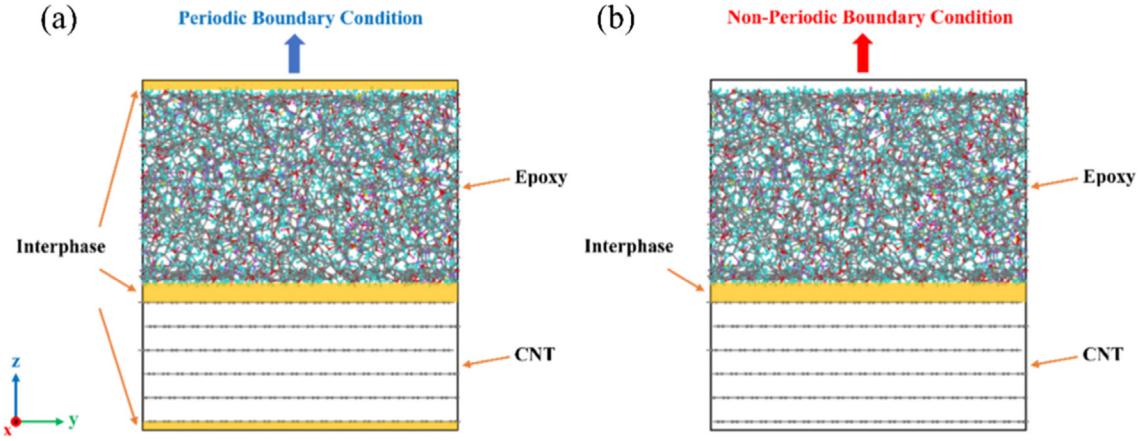

Fig. 6. Sketch of interphase models with (a) periodic boundary conditions and (b) nonperiodic boundary conditions in the z-direction.

2.2.1. Calculation of E_2

When calculating E_2, the model was in a periodic condition, resulting in two interphase layers as illustrated in Fig. 7. The box was stretched in the y-direction at a constant strain rate of 1×10^{-8}. Because only $\varepsilon_y = \Delta W/W$ exists in the interphase, E_2 is calculated as:

$$E_2 = \frac{d^2 U_{inter}}{2V_{inter} d\varepsilon_y{}^2} \tag{3}$$

where V_{inter} denotes the volume of one interphase layer.

2.2.2. Calculation of E_3

When calculating E_3, the nonperiodic condition was implemented in the z-direction, and only one interphase layer was present in the model, as shown in Fig. 8. The motion of the CNTs and epoxy was limited to a rigid body to exclude the deformation of the matrix because the deformation of the matrix should not be included in the interphase response, causing an underestimation of E_3. Subsequently, the CNTs were moved in the z-direction at a velocity of 1×10^{-6} Å/fs. This resulted in the strain $\varepsilon_z = \Delta H/H$ in the interphase, and E_3 was calculated as:

$$E_3 = \frac{d^2 U_{inter}}{V_{inter} d\varepsilon_z{}^2} \tag{4}$$

2.2.3. Calculation of G_{12}

When calculating G_{12}, the periodic condition is implemented in the z-direction. Simple shear loading was performed on the box in the xy-plane, leading to engineering shear strain $\gamma_{xy} = \Delta W/L$ in the interphase layers, as illustrated in Fig. 9. The velocity of the graphene sheets in the z-direction was limited to zero to prevent the graphene sheets from wrinkling during shearing [43]. E_3 is calculated using the following equation:

$$G_{12} = \frac{d^2 U_{inter}}{2V_{inter} d\gamma_{xy}{}^2} \tag{5}$$

2.2.4. Calculation of G_{13}

To calculate G_{13}, a nonperiodic condition was implemented in the z-direction. As illustrated in Fig. 10, a simple shear deformation of the interphase was achieved by moving the CNT in the x-direction. During the moving process, the x-direction velocities of the atoms in the matrix were limited to zero to exclude shear deformation of the matrix, whereas those of the CNT were set as 1×10^{-6} Å/fs. Subsequently, the engineering shearing strain, $\gamma_{xy} = \Delta L/H$ in the interphase was obtained. Finally, G_{13} is calculated using the following equation:

$$G_{13} = \frac{d^2 U_{inter}}{V_{inter} d\gamma_{xz}{}^2} \tag{6}$$

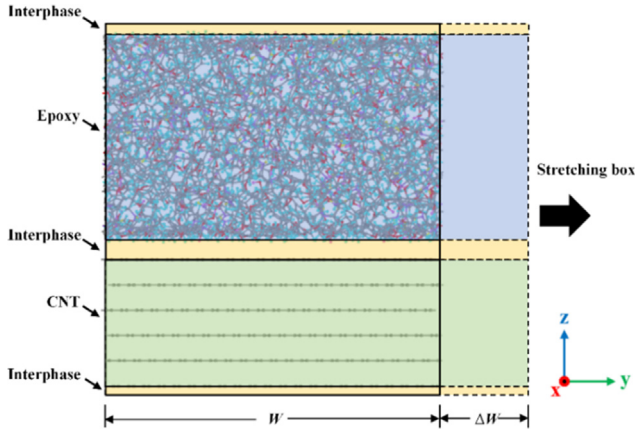

Fig. 7. Sketch of the loading strategy for the calculation of E_2.

3. FEM modelling and simulations

In this study, all FEM simulations of the RVE and shear-lag models were performed using the commercially available ABAQUS software. For comparison, models containing an interphase (interphase model) and those without an interphase (interface model) were developed. The five individual effective elastic constants of the transversely isotropic interphase used in FEM are discussed in **Section 4**. The interphase thickness was 0.3 nm. A type of CNT with a diameter of 2.71 nm and transversely isotropic elastic properties was used [44]. Five effective elastic constants are listed in Table 1. Additionally, by an individual calculation of unreinforced epoxy with MD simulations, the Young's modulus and Poisson's ratio of the isotropic matrix were determined to be 3.17 GPa and 0.34, respectively.

The elastic constants are based on a local Cartesian coordinate system, $x_1x_2x_3$, where the x_3-direction is the elastic axis of symmetry in the CNT's axial direction.

3.1. FEM models of RVE

FEM models of RVE considering perfect interfacial bonding with zero interfacial thickness have been extensively investigated in

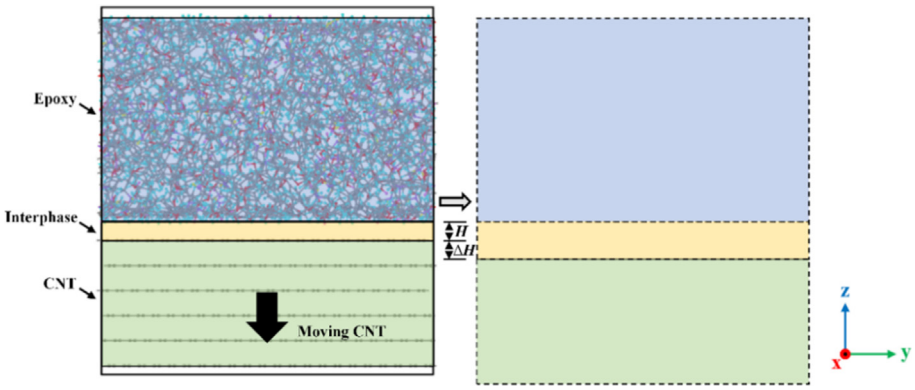

Fig. 8. Sketch of the loading strategy for the calculation of E_3.

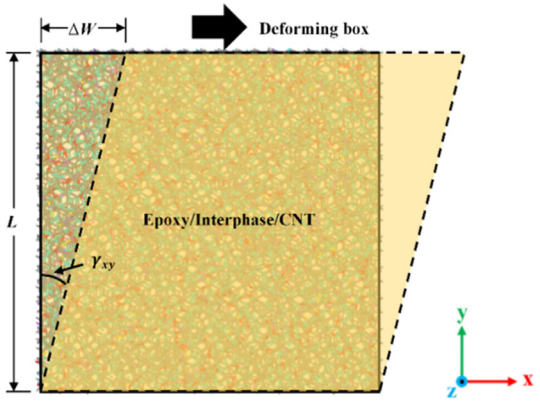

Fig. 9. Sketch of the loading strategy for the calculation of G_{12}.

previous studies [31,45,46]. This simplified role of the interface may result in imprecise load transfer. In our multiscale framework, 3D FEM models of the RVE considering a transversely isotropic interphase were developed in conjunction with the results of MD simulations. Straight CNTs were randomly distributed in the matrix using a master algorithm. Single CNTs were randomly placed in cubic matrix boxes, one by one. Meanwhile, the newly generated CNT were checked for possible intersections with the previously placed CNTs. If any intersection existed, the CNT was deleted and randomly regenerated until no intersection existed. In the interphase models, the interphase surrounded the sidewall of the CNT with uniform thickness. Intersections between interphases did not occur. Moreover, the geometry of the CNTs and interphases was periodic; therefore, parts of the CNTs and interphases protruding beyond the box boundaries reappeared on the opposite boundary. As reported in a previous study [22], a large capillary force was observed between the CNT open end and epoxy. Thus, perfect interfacial bonding between the CNT end and epoxy was assumed.

The transversely isotropic elastic symmetry axis of the interphase is always in the radial direction of the CNT. That is, the symmetry axis varies continuously as the position in the hollow cylinder-shaped interphase continues to change around the CNT axis. The stiffness matrix should vary in the global coordinate system for different positions in the interphase, surrounding different randomly distributed CNTs, via coordinate transformation. To solve this problem, an alternative computation was performed. As illustrated in Fig. 11**a**, the geometry of the interphase is divided into small elements with the same ideal as that explained in **Section 2**. A discrete local Cartesian coordinate system $x_1x_2x_3$ was defined for each cell such that the x_3-axis was the axis of elastic symmetry in the radial direction of the CNT, as shown in Fig. 11**a and b**. The transversely isotropic stiffness matrix, consisting of engineering constants calibrated from MD simulations, can be directly defined on the local coordinate systems. All the developments were implemented based on Python codes embedded in ABAQUS.

Table 1
Five individual elastic constants of transversely isotropic CNTs [44].

E_2(TPa)	E_3(TPa)	G_{12}(TPa)	G_{13}(TPa)	υ_{23}
0.230	0.905	0.08	0.24	0.254

The elastic moduli of the RVE models were calculated at different CNT concentrations (0.5, 1, 1.5, and 2 wt%) and aspect ratios (10, 20, and 30). At least 40 CNTs were placed in all RVE models to ensure a sufficient statistical magnitude, thereby leading to approximately isotropic properties of the RVE models. In addition, the ratios of the RVE edge length to CNT length (L_{RVE}/L_{RVE}) were at least 1.5 to ensure convergence of the elastic properties [47]. Thus, considering the number of CNTs and L_{RVE}/L_{RVE} led to the edge length of the RVE models (L_{RVE}) varying from 67.99 to 155.28 nm. For the tension tests, displacement boundary conditions were imposed to generate a strain of 0.01, by setting uniform displacements in the tension direction on one boundary of the RVE models and zero displacements in the tension direction on the opposite boundary. Moreover, for RVE models at low filler concentrations, the displacement and traction boundary conditions led to close upper and lower bounds for the elastic constants [33]. Therefore, the application of periodic boundary conditions was not essential. The calculated elastic moduli in three different tension directions were averaged.

Linear tetrahedral elements (C3D4) were used because of the complex geometry of RVE models. This is beneficial for a significant increase in computing speed, albeit with a smaller reduction in calculation accuracy compared to quadratic tetrahedral elements (C3D10). Comparison tests were performed, indicating that the differences in the results between them were less than 0.7 %, with approximately 120,000 elements. This type of element was used in another study [32]. As illustrated in Fig. 11**c**, only one element was present in the CNT radial direction of the interphase. This meshing strategy was also used in previous studies [33,48]. The sizes of the elements were near identical for all models, and the number of elements changed based on the size of the RVE. Thus, the number of elements varied from 846,792 to 5784732. Preliminary calculations were made to verify the mesh convergence. By increasing the number of elements by 0.58 times, the results decreased by a small value of 0.052 %. Thus, the mesh converges.

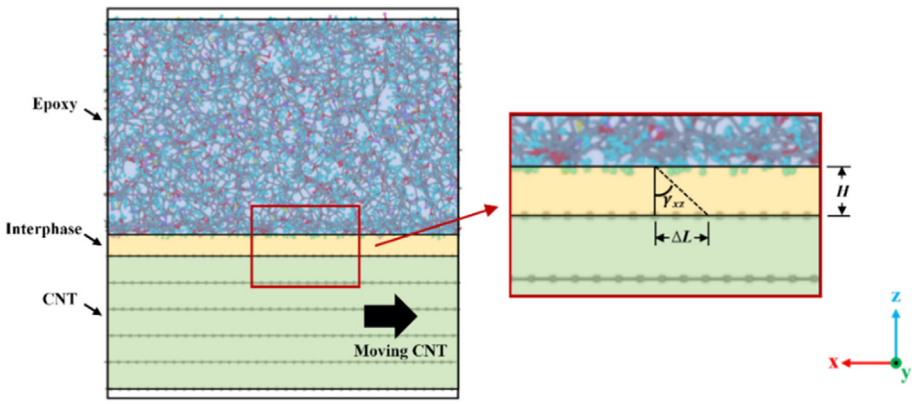

Fig. 10. Sketch of the loading strategy for the calculation of G_{13}.

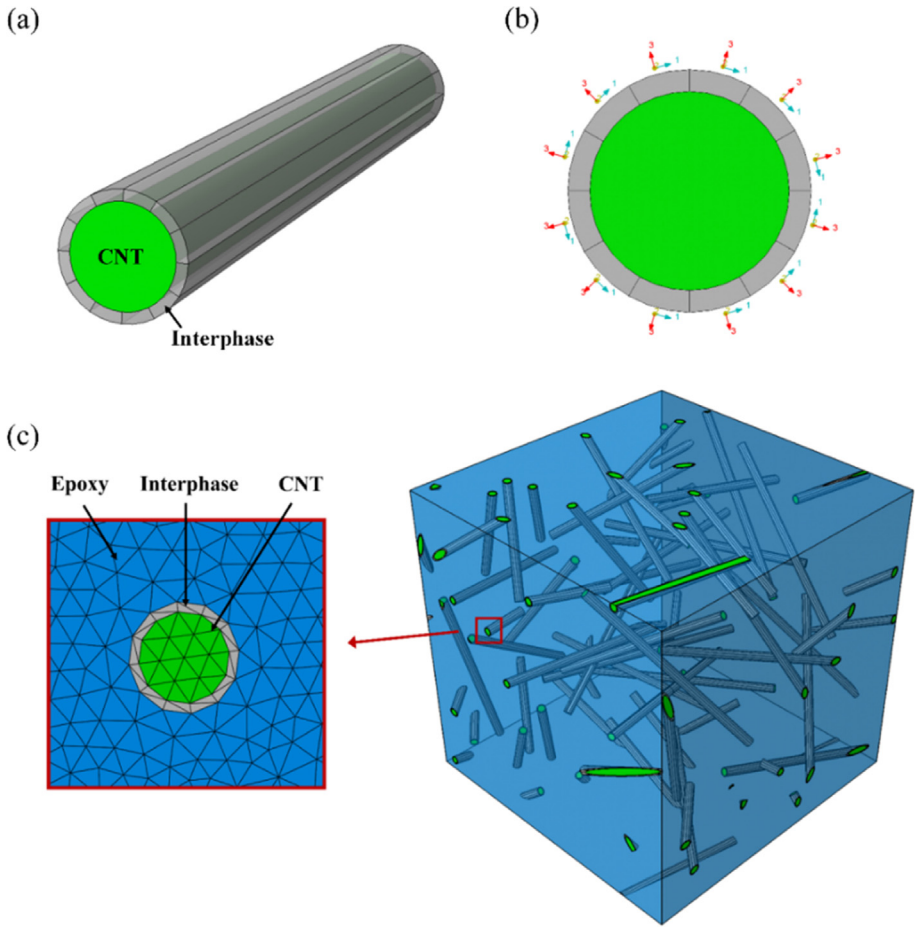

Fig. 11. (a) Structure of interphase, (b) material orientation of interphase, and (c) FEM model of the RVE containing the interphase.

3.2. Shear-lag models of FEM

As shown in Fig. 12, the symmetrical shear-lag model exhibits the shape of a three-phase concentric cylinder. The matrix had a diameter of 2R and length of 2L. The interphase region had a thin shell shape with a diameter of 2b and length of 2l. The CNT had a diameter of 2a and length of 2l. The structure and material definitions of the interphase are identical to those of the RVE models. Perfect interfacial bonding between the CNT end and matrix was assumed. By assuming $a = b$, the interphase model is reduced to the interface model.

For both the interphase and interface models, the matrix-to-CNT diameter ratio (R/a) and matrix-to-CNT length ratio (L/l) were assumed to be 5 and 2, respectively. The axial displacement of the surface on the left side of the model was set at zero, which resulted in symmetrical boundary conditions. A traction boundary condition with an axial normal stress, σ, was applied to the surface on the right side. The aspect ratio of the CNTs was assumed to be 50. Linear triangular prism elements (C3D6) are used in this study. The sweep-mesh method was employed along the z-direction. The mesh used in this section is shown in Fig. 13. Both the interphase and interface models employed the same mesh. Finally, a mesh was generated for each model with 1,485,960 elements. The mesh was denser than that of the RVE and converged.

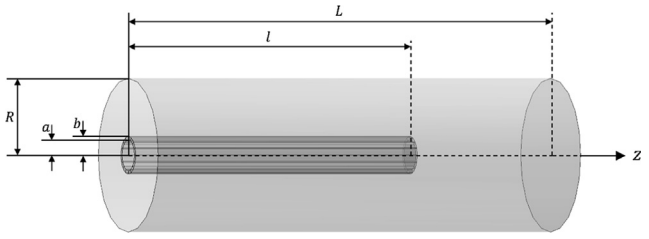

Fig. 12. Scheme of the shear-lag model.

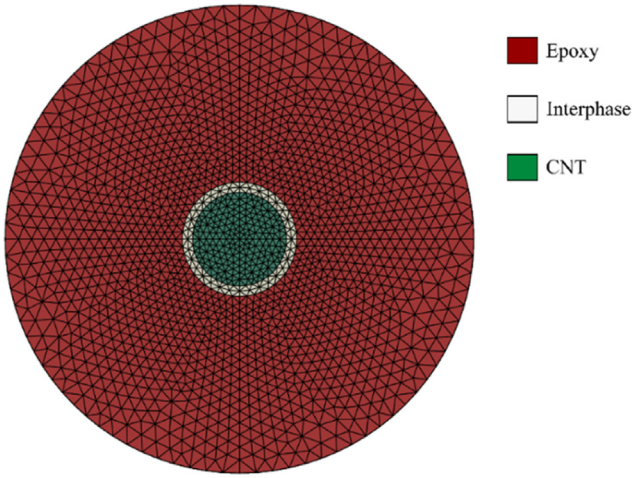

Fig. 13. Mesh on a section perpendicular to the z-direction of the shear-lag for the interphase model case.

4. Results and discussion

4.1. Transversely isotropic elastic properties of CNT-epoxy interphase

In this section, Poisson's ratio (υ_{23}) is assumed to be zero, and four elastic constants are calculated. The variations in the interaction energy density between the CNT and epoxy matrix with a strain increment in the four loading scenarios are discussed. For a linear elastic material, the strain energy density is a quadratic function of the strain. Therefore, the variation in the interaction energy density versus strain was fitted using the following equation:

$$y = Ax^2 + Bx + C \tag{7}$$

where 2*A* is equal to the corresponding engineering modulus in the respective loading scenarios. All elastic constants obtained are summarised in Table 2.

The elastic axis of symmetry is in the z-direction.

4.1.1. e_2

Fig. 14 shows the variation in the interaction energy density versus normal strain, ε_y, from 0 to 0.01 in the loading scenarios described in **Section 2.2.1**. The interaction energy density initially tended to increase quadratically with increasing ε_y from 0 to 0.0065. This can be regarded as the linear-elastic stage of the interphase. Subsequently, the energy density varied without any regularity with increasing ε_y from 0.065 to 0.01, indicating that the interphase exited elasticity. The quadratic variation stage of the interaction energy was fitted, and the in-plane Young's modulus was determined as $E_2 = 362.68$ GPa.

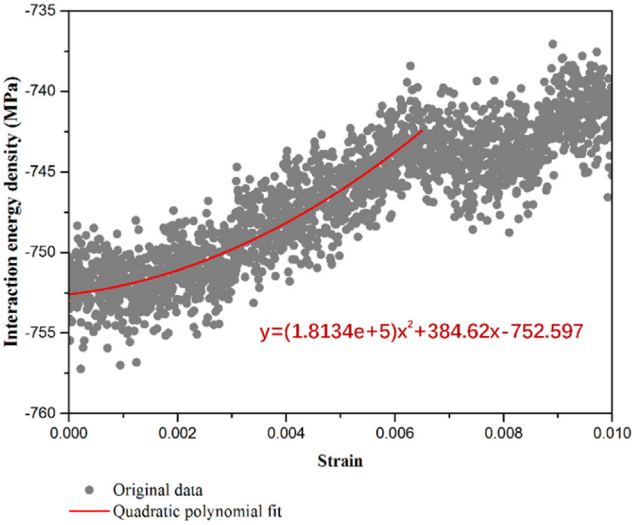

Fig. 14. The variation in the interaction energy density to calculate E_2.

4.1.2. e_3

Fig. 15 shows the variation in the interaction energy density versus the normal strain, ε_z, in the loading scenarios described in **Section 2.2.2**. With ε_z ranging from 0 to 0.01, the interaction energy density increased quadratically, revealing the linear elastic properties of the interphase. By fitting ε_z from 0 to 0.065, the out-of-plane Young's modulus was determined to be $E_3 = 12.19$ GPa. E_3 was higher than the Young's modulus of the matrix. Sahraei et al. [35] performed the same interfacial separation test between graphene and epoxy using MD simulations, except for the rigid body of the matrix. From the snapshots obtained during the test, the deformation of the interphase was significantly smaller than that of the matrix. Damage first occurred in the matrix while the interfacial bonding was intact. This results from $\pi - \pi$ stacking interactions between the benzene rings in the matrix and CNTs. Thus, the value of E_3 in this study was realistic. Moreover, E_3 is an order of magnitude smaller than E_2, exhibiting the inaccuracy of assuming that the interphase is isotropic.

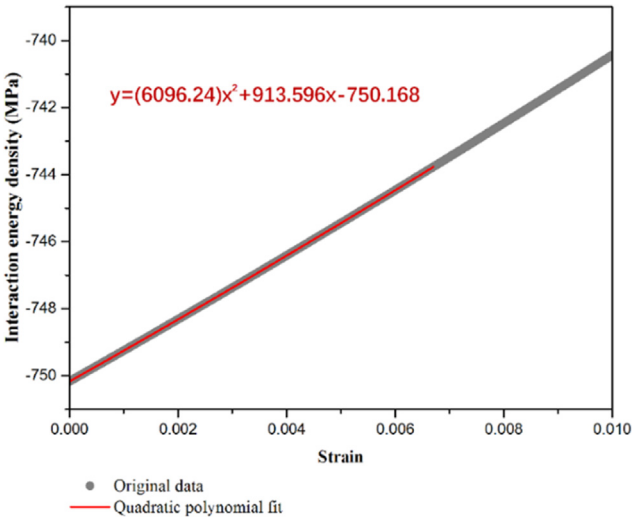

Fig. 15. Variation in the interaction energy density to calculate E_3.

4.1.3. g_{12}

Fig. 16 shows the variation in the interaction energy density versus engineering shear strain, γ_{xy}, from 0 to 0.01, in the loading scenarios described in **Section 2.2.3**. The interaction energy density increases quadratically with increasing γ_{xy} from 0 to 0.005, followed by an irregular variation from 0.005 to 0.01. The two stages indicated that the interphase initially exhibited a linear elastic property and subsequently exited the elastic stage. By fitting the quadratic variation stage of the interaction energy, the in-plane shear modulus was determined to be $G_{12} = 175.08$ GPa.

4.1.4. g_{13}

Fig. 17 shows the variation in the interaction energy density versus engineering shear strain, γ_{xz}, from zero to 0.01 in the loading scenarios described in **Section 2.2.4.** The interaction energy density increased quadratically when increasing γ_{xz} from zero to 0.1, thereby revealing a linear elastic behaviour of the interphase. By fitting the variation in interaction energy, the out-of-plane shear modulus was obtained as $G_{13} = 46.64$ MPa. It can be observed that the value of G_{13} is significantly lower than those of the other mod-

Table 2
Five individual elastic constants of the transversely isotropic interphase.

E_2(GPa)	E_3(GPa)	G_{12}(GPa)	G_{13}(MPa)	υ_{23}
362.68	12.19	175.08	46.64	0

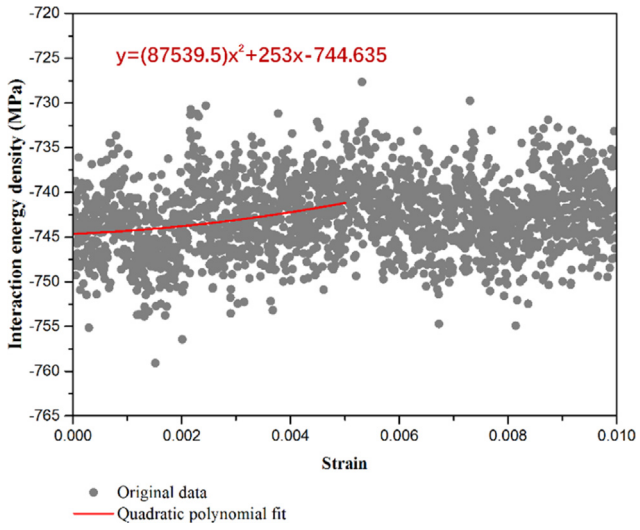

Fig. 16. Variation in the interaction energy density to calculate G_{12}.

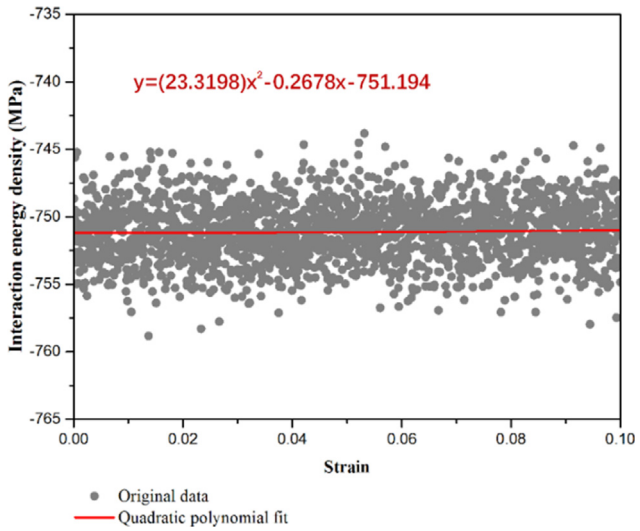

Fig. 17. Variation in interaction energy density to calculate G_{13}.

uli, being four and three orders of magnitude smaller than those of E_2 and E_3, respectively. Moreover, CNTs can be pulled out easier than they can be interfacially separated, which has also been reported in the literature [35].

In addition, the force in the direction of CNT movement can be directly obtained. The interfacial shear stress was calculated as follows:

$$\tau_{interface} = \frac{F}{S} \tag{8}$$

where $\tau_{interface}$, F, and S denote the interfacial shear stress, force on the CNT in the direction of the CNT movement, and cross-sectional area of the graphene sheet, respectively. The force-based $G_{23}{}'$ can then be obtained using:

$$G_{13}{}' = \frac{d\tau_{interface}}{d\gamma_{xz}} \tag{9}$$

Fig. 18 shows the variation in $\tau_{interface}$ versus γ_{xz}. The stress $\tau_{interface}$ increased linearly when increasing γ_{xz} from 0 to 0.1. In this region of γ_{xz}, the stress $\tau_{interface}$ was fitted by a linear equation, and

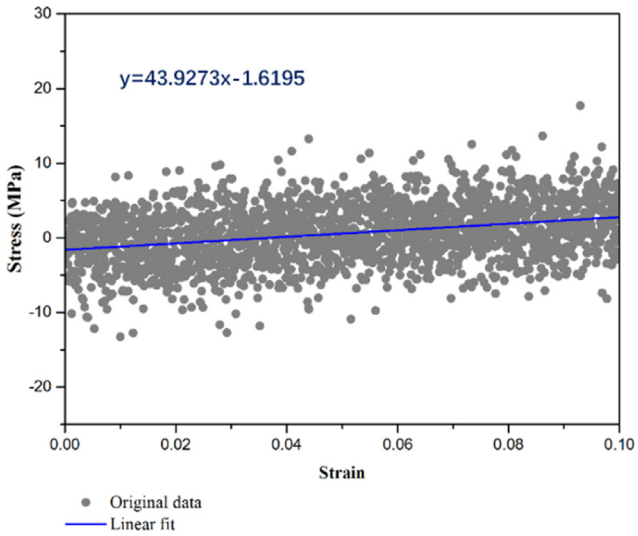

Fig. 18. Variation in the interfacial shear stress $\tau_{interface}$ versus strain γ_{xz}.

the force-based $G_{13}{}'$ was determined as $G_{13}{}' = 43.93$ MPa. It can be observed that the value of $G_{13}{}'$ was only 6.17 % lower than that of G_{13}. Thus, considering that the energy- and force-based methods were completely independent, the moduli calculated based on the interaction energy were confirmed to be precise.

To the best of our knowledge, there has been little research on the interfacial stiffness of nanocomposites, particularly in experiments. Experimental measurements of the interfacial properties were severely hindered by the length scale. However, we can roughly estimate G_{13} from experimental data and MD simulations, in which tests of pulling one CNT out of a matrix were performed. The equation is $G_{13} = \frac{\tau_{IFF} H}{d}$, where τ_{IFF}, d, and H denote the interfacial shear strength, pull-out distance when the interfacial shear stress reaches τ_{IFF}, and thickness of the interphase, respectively. The approximate values of G_{13}, obtained from only one experiment [49] containing sufficient data and one MD simulation test [50], were approximately 0.006 and 97 MPa, respectively. However, because the value of τ_{IFF} in this experiment was lower than in the existing studies and owing to technical limitations and our rough estimation, the G_{13} of this experimental study is far from accurate but can reflect the weak interfacial shear stiffness. In addition, the value of G_{13} from our study was in the range of 0.006–97 MPa and at the same magnitude of 97 Mpa. Thus, the value of G_{13} obtained in the present study was plausible.

4.2. FEM models of RVE

To understand the properties of the composites, the Young's modulus enhancement ratios of the RVE relative to pure epoxy were calculated. Fig. 19 shows the effects of different CNT concentrations and aspect ratios on the enhancement ratios. The enhancement ratios increased with increasing CNT concentrations and aspect ratios. For a low CNT aspect ratio (10), the enhancement ratios of the interphase models were higher than those of the interface models at all concentrations. In contrast, for CNT aspect ratios of 20 and 30, the enhancement ratios of the interphase models were lower than those of the interface model. Table 3 lists various experimental results on enhancement ratios of Young's modulus for CNT/epoxy composites with CNT contents ranging from 0.5 to 1 wt%. It can be observed that the results of our interphase model are in the range of the experimental results but are at a low level in the range. For example, 5.6 % enhancement with CNT aspect ratios of 30 and 0.5 wt% was in the range of 0.38–32.4 % of the experi-

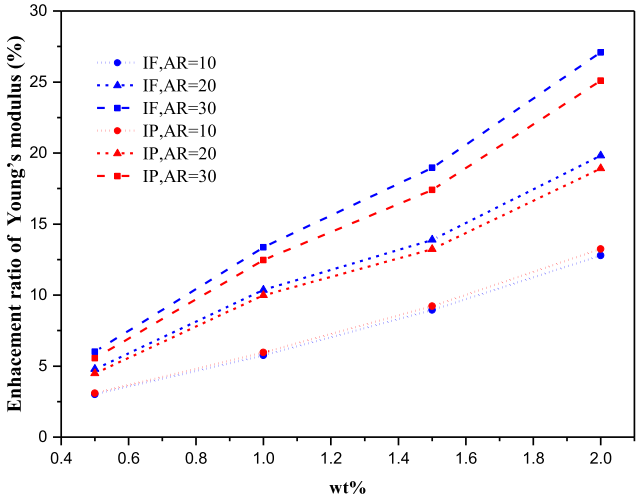

Fig. 19. Enhancement ratios of Young's modulus for RVE models at different concentrations (wt.%) and aspect ratios (AR) of CNT for the interface and interphase models.

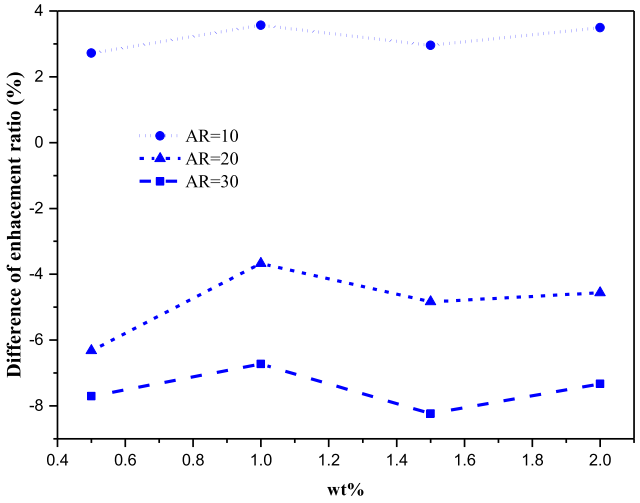

Fig. 20. Differences in enhancement ratio between the interphase and interface models.

Table 3
Comparison of increments in Young's modulus of nanocomposites between various experiments.

Materials	wt.%	Gain in Young's modulus (%)	Reference
EP/MWCNT	0.5	32.4	[51]
EP/DWCNT	0.5	7.349	[52]
EP/MWCNT	0.5	0.38	[52]
EP/MWCNT	0.5	<9	[53]
EP/MWCNT	0.5	0.7	[54]
EP/MWCNT	0.5	13.5	[55]
EP/MWCNT	0.55	20.6	[56]
EP/MWCNT	1	17.4	[51]
EP/MWCNT	1	2.87	[54]
EP/SWCNT	1	18	[57]
EP/MWCNT	1	26.4	[55]

EP, MWCNT, DWCNT, and SWCNT denote epoxy resin, multi-walled CNT, double-wall CNTs, and single-wall CNTs, respectively.

mental results, and 12.47 % with CNT aspect ratios of 30 and 1 wt% was in the range of 2.87–26.4 %. The low value mainly results from the higher CNT aspect ratios in the experiment than those in our simulations. This indicated the applicability of the models used in this study.

For further in-depth studies, the differences in the enhancement ratios between the interphase and interface models were extracted from Fig. 19 and are shown in Fig. 20. From Fig. 20, the differences in the enhancement ratios between the interphase and interface models are evidently not affected by the CNT concentration but are distinctly affected by the CNT aspect ratio. As the aspect ratio increased from 10 to 30, the difference changed from positive to negative. Furthermore, the absolute values of the difference increased with an increase in the aspect ratio (from 20 to 30) after the difference became negative. For example, at a concentration of 2 %, the enhancement ratios of the interphase model were 3.49 % higher and 4.56 and 7.35 % lower than those of the interface model for aspect ratios of 10, 20, and 30, respectively. These phenomena can be explained as follows. Owing to the higher moduli ($E_2, E_3, and\ G_{12}$) of the interphase than that of the epoxy matrix, the interphase can be regarded as an additional reinforcement phase, such as thickening CNTs. That is, the moduli of the interphase induced an enhancement effect on the composites. However, it is worth noting that a low value of G_{13} weakened the load transfer efficiency of the interfacial shear stress. For sufficiently short CNTs, the interfacial load transfer efficiency for interfacial shear stress was not significantly weakened by G_{13}. Thus, the weakening effect of G_{13} is less dominant than that of the other interphase moduli. Finally, considering sufficiently short CNTs, the interphase led to a higher enhancement ratio of the RVE for the interphase model than that for the interface model. Conversely, the interfacial load transfer efficiency for the interfacial shear stress was significantly weakened by G_{13} for longer CNTs. The weakening effect of G_{13} was more evident as the CNT aspect ratio increased, which could not be compensated by the enhancement effect of the other moduli. Therefore, for long CNTs, the interphase led to a lower enhancement ratio of the RVE in the interphase model than in the interface model. The CNT aspect ratio is typically > 100 [58]. Consequently, the interface model led to overestimations of CNT-reinforced composites, which confirms the necessity of using the interphase model proposed in this study.

4.3. Shear-lag models of FEM

The interphase effects on the elastic properties of random CNT-distributed RVE models are described in **Section 4.2**; however, the load transfer mechanism remains unclear. Therefore, the shear-lag models for the interphase and interface were constructed to analyse the effects of the interphase on the load transfer modes. The stress distributed in the shear-lag models was normalised by the axial normal stress, σ, of the traction boundary condition.

Fig. 21 shows the axial normal stress distribution in the shear-lag models. Stress was extracted from the left-end sections of the models. For the interphase model, the maximum stresses of the CNTs, interphase, and matrix are 21.31, 1.04, and 0.07, respectively. For the interface model, the maximum stresses of the CNTs and the matrix were 23.13 and 0.08, respectively. It can be observed that the stress of the CNT is significantly higher than that of the interphase and matrix. In addition, the stress of the interphase was higher than that of the matrix but lower than that of the CNT. Owing to the perfect interfacial bonding between the CNT end and matrix, the stress at the CNT end was not zero. The axial normal stress of the CNT increased in the z-direction owing to the accumulated interfacial shear stress under force equilibration.

For ease of analysis, the normalised average axial normal stress on the CNT is calculated. The normalised interfacial shear stress can then be obtained from:

$$\tau_{inter} = -\frac{1}{2} a \frac{d\sigma_{CNT}}{dz} \tag{10}$$

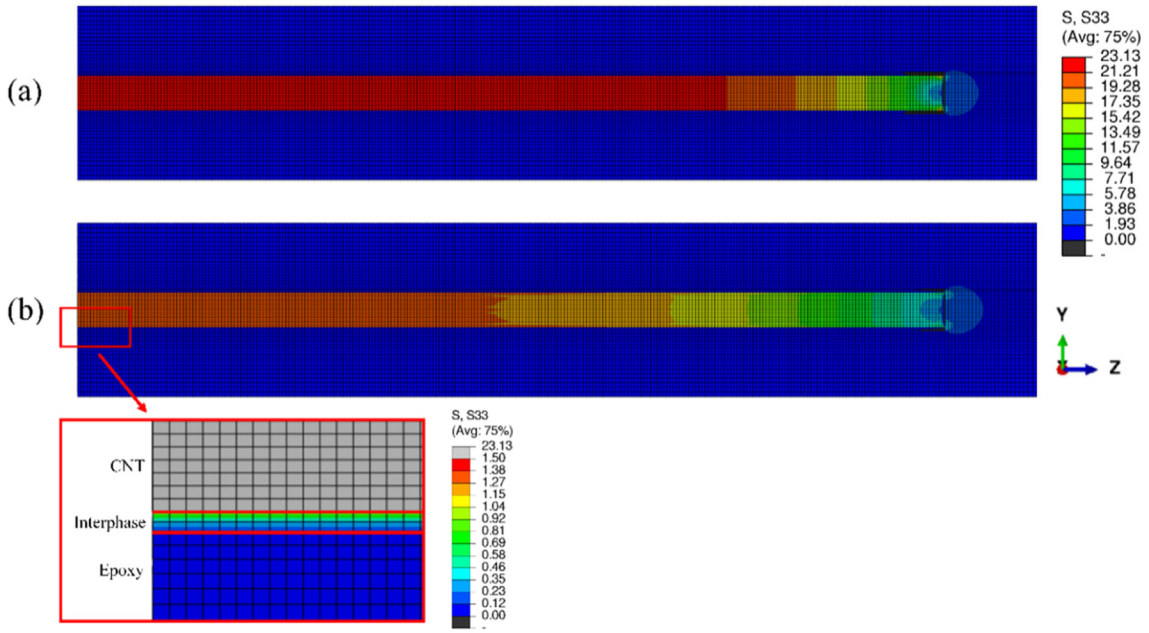

Fig. 21. Sectional drawing of axial normal stress distribution for (a) interface, and (b) interphase models. In this picture, parts of models containing CNTs are shown.

where τ_{inter} denotes the normalised interfacial shear stress and σ_{CNT} denotes the normalised average axial normal stress of the CNT.

Fig. 22**a** shows the average axial normal stress on the CNT. With an increase in $z/2a$, the stress was first evenly distributed in the left region of the CNT and then decreased gradually. The stress of the interphase model was always smaller than that of the interface model. The maximum stress value of 17.76 was obtained from the interphase model, which was 13.64 % lower than the 20.56 of the interphase model. This stems from the higher in-plane Young's modulus (E_2) of the interphase than that of the matrix. Because loads tend to propagate to locations with higher stiffness, the interphase of the interface model bears more axial loads from the matrix and shares part of the axial loads from the CNT compared with the interface model case. In addition, as $z/2a$ increased, the stress of the interphase model decreased slower than that of the interface model, which can be combined with a slower increase in the interfacial shear stress of the interphase model, as shown in Fig. 22**b**. The greatest concern was that the load transfer length (length for which the interfacial shear stress was not zero) of the interphase model was higher than that of the interface model, thereby reducing the effective length bearing the axial load. This was caused by the low out-of-plane shear modulus (G_{13}) of the interphase.

A study by Zhang and He [59] was employed to further clarify the effects of G_{13}. They developed a three-phase shear-lag model with the same geometrical shape. Interestingly, their results exhibited a reverse load-transfer mode. The load transfer length of the interphase model was lower than that of the interface model, which differs from our results. Furthermore, the axial normal stress on the CNT in the interphase model was smaller than that in the interface model, which is consistent with our results. This difference is caused by the Young's modulus of the isotropic interphase being higher than that of the matrix (the shear modulus is higher than that of the matrix), according to Zhang's study, whereas the out-of-plane shear modulus (G_{13}) is lower than that of the matrix, according to our study. Thus, it can be concluded that the low out-of-plane shear modulus (G_{13}) of the interphase increased the load transfer length, leading to a decrease in the efficiency of the load transfer from the matrix to the CNT in our study. This also proves

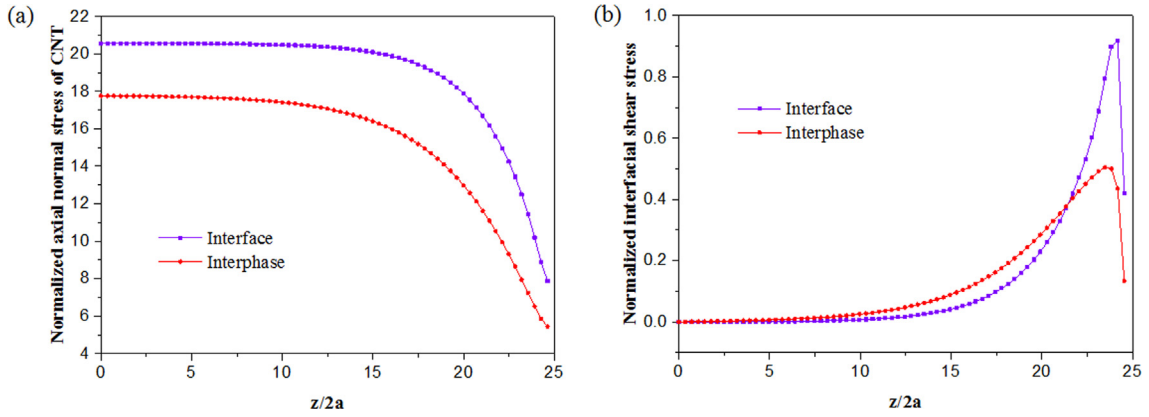

Fig. 22. (a) Average axial normal stress on CNTs, and (b) interfacial shear stress surrounding the CNT.

the mechanism of the reduction in the enhancement ratio in the FEM models of the RVE by introducing an interphase.

5. Conclusions

In this study, a multiscale framework combined with microscale MD and scaled-up FEM RVE-based simulations was proposed to predict the elastic properties of CNT-epoxy composites. First, the interfacial van der Waals interaction region between the CNT and epoxy was assumed to be a transversely isotropic elastic continuum. Four loading scenarios were proposed to calculate the five individual engineering elastic constants based on quadratic fitting of the variation in the interaction energy density versus the specific strain in the MD simulations. The MD simulations results exhibit significant differences between the moduli, from the minimum value of the out-of-plane shear modulus (G_{13} = 46.64 MPa) to the maximum value of the in-plane Young's modulus (E_2 = 362.68 GPa). Subsequently, 3D FEM models of RVE containing a transversely isotropic interphase (interphase model) were developed in conjunction with the results of the MD simulations. The Young's modulus of the interphase model at different concentrations and CNT aspect ratios was calculated and compared to that of the RVE models without an interphase (interface model). The results indicate that the enhancement ratio of the Young's modulus obtained from the interphase model is significantly lower than that obtained from the interface model at high CNT aspect ratios, whereas it is slightly higher than that obtained from the interface model at severely low CNT aspect ratios. Finally, FEM shear-lag models with an interphase were constructed and compared to shear-lag models without an interphase to distinguish the load transfer modes between them. The results indicate that the interphase model has a higher load-transfer distance than the interface model owing to the low value of the out-of-plane shear modulus, G_{13}, of the interphase. Thus, the interphase decreases the efficiency of load transfer from the matrix to the CNT. The framework provides efficient interfacial simulations and a more accurate prediction of bulk elastic properties and can be extended to a wider range of nanocomposites.

Data availability

Data will be made available on request.

Declaration of Competing Interest

The authors declare that they have no known competing financial interests or personal relationships that could have appeared to influence the work reported in this paper.

Acknowledgements

This study was supported by the National Natural Science Foundation of China (Grant No. 51903148) and Guangdong Basic and Applied Basic Research Foundation, China (No. 2021A1515012273). This study was undertaken as a projects (NTF19008, NTF19011) supported by the Start-Up Fund of the Scientific Research at Shantou University, China.

References

[1] P. Gupta, M. Rajput, N. Singla, V. Kumar, D. Lahiri, Electric field and current assisted alignment of CNT inside polymer matrix and its effects on electrical and mechanical properties, Polymer 89 (2016) 119–127.
[2] Y. Li, Q. Wang, S. Wang, A review on enhancement of mechanical and tribological properties of polymer composites reinforced by carbon nanotubes and graphene sheet: Molecular dynamics simulations, Compos. B Eng. 160 (2019) 348–361.
[3] J. Zhang, S. Ye, H. Liu, X. Chen, X. Chen, B. Li, W. Tang, Q. Meng, P. Ding, H. Tian, X. Li, Y. Zhang, P. Xu, J. Shao, 3D printed piezoelectric BNNTs nanocomposites with tunable interface and microarchitectures for self-powered conformal sensors, Nano Energy 77 (2020) 105300.
[4] Wang S, Huang Y, Chang E, Zhao C, Ameli A, Naguib HE, et al. Evaluation and modeling of electrical conductivity in conductive polymer nanocomposite foams with multiwalled carbon nanotube networks. Chemical Engineering Journal. 2021;411:128382.
[5] Rathinavel S, Priyadharshini K, Panda D. A review on carbon nanotube: An overview of synthesis, properties, functionalization, characterization, and the application. Materials Science and Engineering: B. 2021;268:115095.
[6] Y. Zare, K.Y. Rhee, Prediction of tensile modulus in polymer nanocomposites containing carbon nanotubes (CNT) above percolation threshold by modification of conventional model, Curr. Appl Phys. 17 (6) (2017) 873–879.
[7] Y. Zare, K.Y. Rhee, A multistep methodology for calculation of the tensile modulus in polymer/carbon nanotube nanocomposites above the percolation threshold based on the modified rule of mixtures, RSC Adv. 8 (54) (2018) 30986–30993.
[8] S. Fu, Z. Sun, P. Huang, Y. Li, N. Hu, Some basic aspects of polymer nanocomposites: A critical review, Nano Materials Science. 1 (1) (2019) 2–30.
[9] R. Razavi, Y. Zare, K.Y. Rhee, A two-step model for the tunneling conductivity of polymer carbon nanotube nanocomposites assuming the conduction of interphase regions, RSC Adv. 7 (79) (2017) 50225–50233.
[10] Y. Zare, K.Y. Rhee, Multistep modeling of Young's modulus in polymer/clay nanocomposites assuming the intercalation/exfoliation of clay layers and the interphase between polymer matrix and nanoparticles, Compos. A Appl. Sci. Manuf. 102 (2017) 137–144.
[11] J. Shen, W. Huang, L. Wu, Y. Hu, M. Ye, The reinforcement role of different amino-functionalized multi-walled carbon nanotubes in epoxy nanocomposites, Compos. Sci. Technol. 67 (15-16) (2007) 3041–3050.
[12] Y. Zare, Study on interfacial properties in polymer blend ternary nanocomposites: Role of nanofiller content, Comput. Mater. Sci. 111 (2016) 334–338.
[13] Y. Zare, A. Daraei, M. Vatani, P. Aghasafari, An analysis of interfacial adhesion in nanocomposites from recycled polymers, Comput. Mater. Sci. 81 (2014) 612–616.
[14] Y. Zare, K.Y. Rhee, Development of Hashin-Shtrikman model to determine the roles and properties of interphases in clay/CaCO3/PP ternary nanocomposite, Appl. Clay Sci. 137 (2017) 176–182.
[15] Y. Zare, Modeling approach for tensile strength of interphase layers in polymer nanocomposites, J. Colloid Interface Sci. 471 (2016) 89–93.
[16] W. Peng, S. Rhim, Y. Zare, K.Y. Rhee, Effect of "Z" factor for strength of interphase layers on the tensile strength of polymer nanocomposites, Polym. Compos. 40 (3) (2019) 1117–1122.
[17] Y. Zare, K.Y. Rhee, Dependence of Z Parameter for Tensile Strength of Multi-Layered Interphase in Polymer Nanocomposites to Material and Interphase Properties, Nanoscale Res. Lett. 12 (2017) 42.
[18] Y. Zare, K.Y. Rhee, Tensile modulus prediction of carbon nanotubes-reinforced nanocomposites by a combined model for dispersion and networking of nanoparticles, J. Mater. Res. Technol. 9 (1) (2020) 22–32.
[19] Y. Zare, M. Fasihi, K.Y. Rhee, Efficiency of stress transfer between polymer matrix and nanoplatelets in clay/polymer nanocomposites, Appl. Clay Sci. 143 (2017) 265–272.
[20] Q.L. Xiong, S.A. Meguid, Atomistic investigation of the interfacial mechanical characteristics of carbon nanotube reinforced epoxy composite, Eur. Polym. J. 69 (2015) 1–15.
[21] Q. Lv, Z. Wang, S. Chen, C. Li, S. Sun, S. Hu, Effects of single adatom and Stone-Wales defects on the elastic properties of carbon nanotube/polypropylene composites: A molecular simulation study, Int. J. Mech. Sci. 131–132 (2017) 527–534.
[22] Z. Song, Y. Li, B. Yang, The interfacial load-transfer enhancement mechanism of amino-functionalised carbon nanotube reinforced epoxy matrix composites: A molecular dynamics study, Compos. Sci. Technol. 209 (2021).
[23] D. Savvas, G. Stefanou, V. Papadopoulos, M. Papadrakakis, Effect of waviness and orientation of carbon nanotubes on random apparent material properties and RVE size of CNT reinforced composites, Compos. Struct. 152 (2016) 870–882.
[24] S.M. Rahimian-Koloor, S.M. Hashemianzadeh, M.M. Shokrieh, Effect of CNT structural defects on the mechanical properties of CNT/Epoxy nanocomposite, Physica B 540 (2018) 16–25.
[25] Y. Li, S. Wang, Q. Wang, M. Xing, Enhancement of fracture properties of polymer composites reinforced by carbon nanotubes: A molecular dynamics study, Carbon 129 (2018) 504–509.
[26] T. Gates, G. Odegard, S. Frankland, T. Clancy, Computational materials: Multi-scale modeling and simulation of nanostructured materials, Compos. Sci. Technol. 65 (15-16) (2005) 2416–2434.
[27] Q.H. Zeng, A.B. Yu, G.Q. Lu, Multiscale modeling and simulation of polymer nanocomposites, Prog. Polym. Sci. 33 (2) (2008) 191–269.
[28] S. Kundalwal, M. Ray, S. Meguid, Shear lag model for regularly staggered short fuzzy fiber reinforced composite, J. Appl. Mech. 81 (2014).
[29] S.I. Kundalwal, S.A. Meguid, Micromechanics modelling of the effective thermoelastic response of nano-tailored composites, Eur. J. Mech. A. Solids 53 (2015) 241–253.
[30] A.R. Alian, S.I. Kundalwal, S.A. Meguid, Interfacial and mechanical properties of epoxy nanocomposites using different multiscale modeling schemes, Compos. Struct. 131 (2015) 545–555.

[31] S. Doagou-Rad, J.S. Jensen, A. Islam, L. Mishnaevsky, Multiscale molecular dynamics-FE modeling of polymeric nanocomposites reinforced with carbon nanotubes and graphene, Compos. Struct. 217 (2019) 27–36.
[32] F. Zaccardi, M.G. Santonicola, S. Laurenzi, Role of interface bonding on the elastic properties of epoxy-based nanocomposites with carbon nanotubes using multiscale analysis, Compos. Struct. 255 (2021).
[33] J. Fankhänel, B. Arash, R. Rolfes, Elastic interphase properties of nanoparticle/epoxy nanocomposites: A molecular dynamics study, Engineering, Composites Part B, 2019, p. 176.
[34] B. Arash, Q. Wang, V.K. Varadan, Mechanical properties of carbon nanotube/polymer composites, Sci. Rep. 4 (2014) 6479.
[35] A. Alizadeh Sahraei, A. Hadi Mokarizadeh, M. Foroutan, D. George, D. Rodrigue, M. Baniassadi, Atomistic simulation of interfacial properties and damage mechanism in graphene nanoplatelet/epoxy composites, Comput. Mater. Sci. 184 (2020).
[36] Y. Li, N. Hu, G.o. Yamamoto, Z. Wang, T. Hashida, H. Asanuma, C. Dong, T. Okabe, M. Arai, H. Fukunaga, Molecular mechanics simulation of the sliding behavior between nested walls in a multi-walled carbon nanotube, Carbon 48 (10) (2010) 2934–2940.
[37] B. Coto, I. Antia, J. Barriga, M. Blanco, J.-R. Sarasua, Influence of the geometrical properties of the carbon nanotubes on the interfacial behavior of epoxy/CNT composites: A molecular modelling approach, Comput. Mater. Sci. 79 (2013) 99–104.
[38] A.P. Awasthi, D.C. Lagoudas, D.C. Hammerand, Modeling of graphene–polymer interfacial mechanical behavior using molecular dynamics, Modell. Simul. Mater. Sci. Eng. 17 (2009).
[39] M. Li, H. Zhou, Y. Zhang, Y. Liao, H. Zhou, The effect of defects on the interfacial mechanical properties of graphene/epoxy composites, RSC Adv. 7 (73) (2017) 46101–46108.
[40] Li Y, Seidel GD. Multiscale modeling of the effects of nanoscale load transfer on the effective elastic properties of unfunctionalized carbon nanotube–polyethylene nanocomposites. Modelling & Simulation in Materials Science & Engineering. 2015;22:025023.
[41] Y. Zhang, X. Zhuang, J. Muthu, T. Mabrouki, M. Fontaine, Y. Gong, T. Rabczuk, Load transfer of graphene/carbon nanotube/polyethylene hybrid nanocomposite by molecular dynamics simulation, Compos. B Eng. 63 (2014) 27–33.
[42] W. Jian, D. Lau, Understanding the effect of functionalization in CNT-epoxy nanocomposite from molecular level, Compos. Sci. Technol. 191 (2020).
[43] W.H. Duan, K. Gong, Q. Wang, Controlling the formation of wrinkles in a single layer graphene sheet subjected to in-plane shear, Carbon 49 (9) (2011) 3107–3112.
[44] S.I. Kundalwal, V. Choyal, Transversely isotropic elastic properties of carbon nanotubes containing vacancy defects using MD, Acta Mech. 229 (6) (2018) 2571–2584.
[45] A. Chanteli, K.I. Tserpes, Finite element modeling of carbon nanotube agglomerates in polymers, Compos. Struct. 132 (2015) 1141–1148.
[46] R. Doles, S.H.R. Sanei, Representative Volume Element for Mechanical Properties of Carbon Nanotube Nanocomposites Using Stochastic Finite Element Analysis, J. Eng. Mater. Technol. 142 (2020).
[47] A.R. Alian, S.A. Meguid, Large-scale atomistic simulations of CNT-reinforced thermoplastic polymers, Compos. Struct. 221–30 (2018).
[48] A. Almasi, M. Silani, H. Talebi, T. Rabczuk, Stochastic analysis of the interphase effects on the mechanical properties of clay/epoxy nanocomposites, Compos. Struct. 133 (2015) 1302–1312.
[49] Y. Ganesan, C. Peng, Y. Lu, P.E. Loya, P. Moloney, E. Barrera, B.I. Yakobson, J.M. Tour, R. Ballarini, J. Lou, Interface toughness of carbon nanotube reinforced epoxy composites, ACS Appl. Mater. Interfaces 3 (2) (2011) 129–134.
[50] R. Rafiee, A. Ghorbanhosseini, Investigating interaction between CNT and polymer using cohesive zone model, Polym. Compos. 39 (11) (2018) 3903–3911.
[51] A. Hameed, M. Islam, I. ahmad, N. Mahmood, S. Saeed, H. Javed, Thermal and mechanical properties of carbon nanotube/epoxy nanocomposites reinforced with pristine and functionalized multiwalled carbon nanotubes, Polym. Compos. 36 (10) (2015) 1891–1898.
[52] F. Gojny, M. Wichmann, B. Fiedler, K. Schulte, Influence of different carbon nanotubes on the mechanical properties of epoxy matrix composites – A comparative study, Compos. Sci. Technol. 65 (15-16) (2005) 2300–2313.
[53] Q.u. Zehua, W. Guojian, A comparative study on the properties of the different amino-functionalized multiwall carbon nanotubes reinforced epoxy resin composites, J. Appl. Polym. Sci. 124 (1) (2012) 403–411.
[54] L.-C. Tang, H. Zhang, J.-H. Han, X.-P. Wu, Z. Zhang, Fracture mechanisms of epoxy filled with ozone functionalized multi-wall carbon nanotubes, Compos. Sci. Technol. 72 (1) (2011) 7–13.
[55] P. Smolen, T. Czujko, Z. Komorek, D. Grochala, A. Rutkowska, M. Osiewicz-Powezka, Mechanical and Electrical Properties of Epoxy Composites Modified by Functionalized Multiwalled Carbon Nanotubes, Materials (Basel) 14 (2021).
[56] K. Alasvand Zarasvand, H. Golestanian, Determination of nonlinear behavior of multi-walled carbon nanotube reinforced polymer: Experimental, numerical, and micromechanical, Mater. Des. 109 (2016) 314–323.
[57] L. Sun, G.L. Warren, J.Y. O'Reilly, W.N. Everett, S.M. Lee, D. Davis, D. Lagoudas, H.-J. Sue, Mechanical properties of surface-functionalized SWCNT/epoxy composites, Carbon 46 (2) (2008) 320–328.
[58] M. Rahmandoust, M.R. Ayatollahi, Characterization of Carbon Nanotube Based Composites under Consideration of Defects, Advanced Structured Materials. 39 (2016).
[59] J. Zhang, C. He, A three-phase cylindrical shear-lag model for carbon nanotube composites, Acta Mech. 196 (1-2) (2008) 33–54.